Structural Analysis of a Chimeric Bacterial α-Amylase. High-Resolution Analysis of Native and Ligand Complexes[†,‡]

Andrzej M. Brzozowski,[§] David M. Lawson,[§,||] Johan P. Turkenburg,[§] Henrik Bisgaard-Frantzen,[⊥] Allan Svendsen,[⊥] Torben V. Borchert,[⊥] Zbigniew Dauter,[§,#] Keith S. Wilson,[§] and Gideon J. Davies*[,§]

Department of Chemistry, Structural Biology Laboratory, University of York, Heslington, York YO10 5DD, U.K., and Novo Nordisk A/S, Novo Alle, DK-2880 Bagsvaerd, Denmark

Received January 7, 2000; Revised Manuscript Received April 26, 2000

ABSTRACT: Several chimeric α-amylases genes were constructed by an in vivo recombination technique from the *Bacillus amyloliquefaciens* and *Bacillus licheniformis* genes. One of the fusion amylases (hereafter BA2), consisting of residues 1−300 from *B. amyloliquefaciens* and 301−483 from *B. licheniformis*, has been extensively studied by X-ray crystallography at resolutions between 2.2 and 1.7 Å. The 3-dimensional structure of the native enzyme was solved by multiple isomorphous replacement, and refined at a resolution of 1.7 Å. It consists of 483 amino acids, organized similarly to the known *B. lichiniformis* α-amylase structure [Machius et al. (1995) *J. Mol. Biol. 246*, 545−559], but features 4 bound calcium ions. Two of these form part of a linear cluster of three ions, the central ion being attributed to sodium. This cluster lies at the junction of the A and B domains with one calcium of the cluster structurally equivalent to the major Ca^{2+} binding site of fungal α-amylases. The third calcium ion is found at the interface of the A and C domains. BA2 contains a fourth calcium site, not observed in the *B. licheniformis* α-amylase structure. It is found on the C domain where it bridges the two β-sheets. Three acid residues (Glu261, Asp328, and Asp231) form an active site similar to that seen in other amylases. In the presence of TRIS buffer, a single molecule of TRIS occupies the −1 subsite of the enzyme where it is coordinated by the three active-center carboxylates. Kinetic data reveal that BA2 displays properties intermediate to those of its parents. Data for crystals soaked in maltooligosaccharides reveal the presence of a maltotriose binding site on the N-terminal face of the $(\beta/\alpha)_8$ barrel of the molecule, not previously described for any α-amylase structure, the biological function of which is unclear. Data for a complex soaked with the tetrasaccharide inhibitor acarbose, at 1.9 Å, reveal a decasaccharide moiety, spanning the −7 to +3 subsites of the enzyme. The unambiguous presence of three unsaturated rings in the $^2H_3$ half-chair/^2E envelope conformation, adjacent to three 6-deoxypyranose units, clearly demonstrates synthesis of this acarbose-derived decasaccharide by a two-step transglycosylation mechanism.

α-Amylases (1,4-α-glucan 4-glucanohydrolase; EC 3.2.1.1) are ubiquitous enzymes which catalyze the breakdown of amylose and amylopectin through the hydrolysis of internal α-1,4-glycosidic linkages with net retention of anomeric configuration. Together with many other enzymes that work on α-linked glucopyranose-derived substrates, such as α-glucosidases, cyclodextrin glycosyltransferases (CGTases),[1] and pullulanases, they are found in family 13 of the glycoside hydrolase sequence-classification, often termed the "α-amylase" superfamily (*1*−*3*). The three-dimensional structures for numerous members of this family have been determined, including the α-amylases from *Aspergillus oryzae* (*4*), *Aspergillus niger* (*5*), porcine pancreas (*6*), barley (*7*), human saliva (*8*), *Bacillus licheniformis* (*9*), *Bacillus stearothermophilus* (*10*), and *Alteromonas haloplanctis* (*11*, *12*). Structures of a number of CGTases and their complexes have also been reported (for example, see refs *13*−*17*).

A feature common to all these reported structures is their $(\beta/\alpha)_8$ catalytic core domain, termed domain A. An excursion between barrel strand β-3 and helix α-3 forms the B domain, while the C domain, frequently an eight-stranded β-sheet, lies at the C-terminal extremity of the barrel. Some family members may contain additional domains, with the CGTases and the *B. stearothermophilus* α-amylase existing as five domain structures with some of the additional domains implicated in binding to granular starch (*10*, *15*, *16*). The α-amylase family domain arrangement and protein engineering have recently been reviewed (*18*, *19*). All family 13 members possess a constellation of three acidic residues, located at the C-terminal face of the $(\beta/\alpha)_8$-barrel, which

[†] This work was supported by the Biotechnology and Biological Sciences Research Council and Novo-Nordisk A/S. Data collection was supported by the EU TMR/LSF program. G.J.D. is a Royal Society University Research Fellow.

[‡] Coordinates for the structure described in this paper have been deposited with the Protein Data Bank (accession numbers 1e3x, 1e3z, 1e4φ, and 1e43).

* Corresponding author. Telephone number +44-(0)1904-432596; Fax number -44-1904-410519; email davies@ysbl.york.ac.uk.

[§] University of York.

[||] Present address: Nitrogen Fixation Laboratory, John Innes Centre, Norwich Research Park, Norwich, NR4 7UH, U.K.

[⊥] Novo Nordisk A/S.

[#] Present address: Brookhaven National Laboratory, Building 725A-X9, Upton, NY 11973.

[1] Abbreviations: BLA, *Bacillus licheniformis* α-amylase; BAA, *Bacillus amyloliquefaciens* α-amylase; BA2, chimeric α-amylase consisting of residues 1−300 from *B. amyloliquefaciens* and 301−483 from *B. licheniformis*); CGTase, cyclodextrin glucosyltransferase.

10.1021/bi0000317 CCC: $19.00
Published on Web 07/14/2000

are implicated in catalysis. α-Amylases perform catalysis with net retention of anomeric configuration in a double-displacement mechanism (*20*). The mechanism involves the formation, and subsequent breakdown, of a covalent glycosyl-enzyme intermediate via oxocarbenium-ion like transition states (for a review, see *19*). One of the residues of the catalytic triad functions as the catalytic nucleophile while another functions as the catalytic acid/base. The catalytic nucleophile has been trapped and identified with 2,2-difluoro and 5-fluoro sugars (*21, 22*) and through the use of mutated proteins (*23*). This latter approach has recently been used to analyze the 3-D structure of the covalent glycosyl-enzyme intermediate of CGTase (*17*).

α-Amylase family members find widespread use in a diverse array of industrial processes ranging from the breakdown of starch to glucose-syrups through to the production of cyclodextrins for the pharmaceutical industry. Many strategies have been used to generate new, more effective, amylases for these processes. In this paper we describe the construction of a chimeric α-amylase, termed BA2, which is formed by the fusion of two bacterial α-amylase genes encoding residues 1−300 from the *B. amyloliquefaciens* α-amylase and residues 301−483 from the *B. licheniformis* enzyme. The three-dimensional structure of BA2 has been solved by multiple isomorphous replacement and refined at a resolution of 1.7 Å. The structure of BA2 in complex with acarbose, at 1.9 Å resolution, reveals a decasaccharide species bound through the −7 to +3 subsites of the enzyme, while structures in the presence of maltooligosaccharides reveal a previously undescribed maltodextrin binding site on the N-terminal face of the $(\beta/\alpha)_8$ barrel.

EXPERIMENTAL PROCEDURES

Crystallization, MIR Data Collection, and Structure Solution. The chimeric gene encoding the BA2 amylase was constructed by an in vivo recombination method. The point of recombination was determined by DNA sequencing. The ambiguity of its location is caused by the amino acid sequence identity between BAM and BLA in the crossover region. The N-terminal portion of the chimeric enzyme is derived from the *Bacillus amyloliquefaciens* α-amylase (residues 1−300), and the C-terminal section from the *Bacillus licheniformis* α-amylase (residues 301−483).

BA2 was crystallized at 18 °C by hanging-drop vapor diffusion using 8−13% (w/v) of either monomethyl ether poly(ethylene glycol) 2000 or 5000 as precipitant. Hanging-drops were buffered with 0.1 M Tris/HCl, pH 7.5 or pH 10.0, containing 5 mM $CaCl_2$, and the protein concentration was in the range 30−35 mg mL^{-1}. Large crystals grew after several days from an amorphous precipitate which formed shortly after setting up the experiment. The crystals had a tendency to grow as clusters, which could usually be separated into single crystals by careful manipulation. Isomorphous derivatives were prepared by transferring crystals to the appropriate mother liquor containing low concentrations of heavy atom compounds. Crystals for maltooligosaccharide and acarbose complexes were grown exactly as for the native enzyme structure and then soaked with the appropriate oligosaccharide at a concentration of 10 mM.

BA2 crystals are in the orthorhombic space group $C222_1$ with approximate cell dimensions $a = 52.7$ Å, $b = 78.3$ Å, $c = 238.7$ Å. To minimize the recording of overlapping reflections during data collection, the *c*-axis was always aligned with the rotation axis, with a 5−10° offset used to minimize loss of data in the "blind-region". X-ray data were collected either in-house using a Rigaku RAXIS IIC image plate system and a RU200HB copper rotating anode, or on station X-11 at EMBL Hamburg outstation using a MAR-Research imaging plate, or on station PX9.5 at Daresbury also using a MAR-Research imaging plate. All data were processed and reduced with the HKL suite of programs (*24, 25*). All subsequent processing used programs from the CCP4 suite unless otherwise stated (*26*).

At the time of structure solution, there were no homologous bacterial α-amylase coordinates available for structure solution by molecular replacement. The structure was therefore solved by multiple isomorphous replacement (MIR). Data on six heavy atom derivatives were collected at 3.0 Å resolution. A single-site gold derivative [potassium dicyanoaurate(I)] yielded a readily interpretable isomorphous difference Patterson (not shown). All subsequent derivatives were solved and brought to a common origin by inspection of cross-Fourier difference maps phased on these SIR_{Au} phases. The gold derivative data were subsequently recollected to 2.2 Å. The final set of experimental phases had an overall figure-of-merit of 0.73 to 2.2 Å. Map quality was improved using DM (*27*); the map was skeletonized and model building was performed using the program O (*28*). Five percent of the observations were set aside for cross-validation analysis (*29*) and used to monitor various refinement strategies and as the basis for maximum-likelihood refinement using REFMAC (*30*). The same set of cross-validation reflections was maintained for the refinement of all subsequent complexes.

High-Resolution Native Data. Data were collected at the European Synchrotron Radiation Facility (ESRF) beamline ID 14-4 at a wavelength of 0.9836 Å. An ADSC QUAD-4 CCD was used as detector. Crystals were mounted in Rayon fiber loops and immediately placed in a stream of boiling N_2 gas at 100 K. Data were collected to a resolution of 1.7 Å with an oscillation range of 0.3°/image. The structures were refined, as outlined above, with the addition that at 1.7 Å hydrogen scattering from "riding" hydrogen atoms was included as a fixed contribution as justified by a drop in R and R_{free} of 2.1/2.0%.

Activity Assays. The activities of the BA2 chimera and its two parent amylases were analyzed as a function of pH over the range pH 4.0−10.5 using the Phadebas α-amylase test kit (Pharmacia). Measurements were carried out at 37 °C in 50 mM Britton−Robinson buffer containing 0.1 mM $CaCl_2$, as described previously (*31*). This assay is based upon the use of a blue-colored insoluble starch as substrate, which releases blue color into the solution upon cleavage. Hydrolysis was stopped by adding one-sixth volume of 1 M NaOH to the reaction mixture. Unhydrolyzed blue starch was removed by filtration. The amount of hydrolyzed substrate is proportional to the absorbance at 620 nm, and activity measurements obtained by this method can be regarded as an apparent k_{cat} for insoluble starch. In a second series of experiments, the activities of the chimera and its parents were assayed as a function of temperature from 37 to 90 °C.

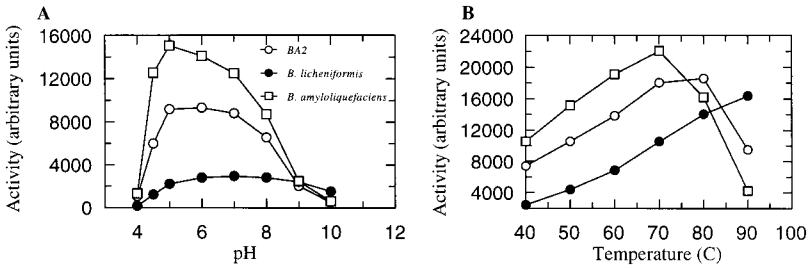

FIGURE 1: Kinetic comparison of the BA2 amylase with its parent enzymes. (A) pH−activity profile. (B) Temperature−activity profile.

Table 1: Data and Structure Refinement Statistics for BA2 Amylase

	native	acarbose	Tris/maltotriose	pH 10
data				
X-ray source	EMBL	EMBL	Cu Kα	ESRF
temp (K)	289	289	289	100
resolution	15−1.92 Å (1.96−1.92 Å)	15−1.93 Å (1.96−1.93 Å)	15−2.2 Å (2.3−2.2 Å)	15−1.7 Å (1.76−1.70 Å)
R_{merge} (outer bin)	0.12 (0.19)	0.07 (0.13)	0.050 (0.089)	0.070 (0.081)
completeness (%)	99 (98)	100 (99)	94 (77)	98 (99)
multiplicity	4.6 (3.4)	4.1 (3.5)	5.2 (4.6)	3.0 (3.1)
I/σ	13 (7)	16 (10)	33 (13)	15 (13)
refinement				
R_{cryst} (R_{free})	0.14 (0.20)	0.13 (0.19)	0.13 (0.21)	0.13 (0.18)
1−2 bonds (Å)	0.011	0.010	0.010	0.010
1−3 angle distance (Å)	0.030	0.026	0.030	0.026
planes (Å)	0.010	0.010	0.010	0.012
chiral volumes (Å^3)	0.122	0.126	0.122	0.100
mean *B* protein (Å^2)	13.0	12.1	13.9	10.2
mean *B* ligands (Å^2)	N/A	16.1	32.6	N/A

RESULTS AND DISCUSSION

Several chimeric α-amylase genes had previously been constructed by in vivo recombination technique using the *Bacillus amyloliquefaciens* and *Bacillus licheniformis* genes. One of the fusion amylase constructs, consisting of residues 1−300 from *B. amyloliquefaciens* and 301−483 from *B. licheniformis*, was termed "BA2". Its functional properties were analyzed, and its structure was analyzed by X-ray crystallography.

BA2 displays a specific activity of approximately 9700 units/mg using the Phadebas assay on "blue" starch (as described in ref *31*). This is intermediate between the values displayed by each of its parents using this assay: 7500 and 30 000 units/mg for the *B. licheniformis* and *B. amyloliquefaciens* enzymes, respectively. For all other properties tested, BA2 is also intermediate in behavior compared to its parents and is generally more similar to the *B. amyloliquefaciens* enzyme. BA2 displays an approximately bell-shaped pH profile with acid and basic limbs exhibiting pK_a's of approximately 4.4 and 8.3, respectively. While interpretation of simple pH−activity curves is fraught with danger, we assume that the acidic limb reflects the pK_a of the catalytic nucleophile, Asp231, although components of stability cannot be ruled out (described more completely for the *B. licheniformis* enzyme in ref *31*). The two parents show similar profiles, although the *B. licheniformis* enzyme maintains activity at higher pH values (pK_a for the basic limb is approximately 10) (Figure 1A). The temperature−activity profile likewise reveals that the behavior of BA2 is most similar to the *B. amyloliquefaciens* enzyme. BA2 shows a higher temperature optimum than the *B. amyloliquefaciens* enzyme, 80 as opposed to 70 °C, while the *B. licheniformis* enzyme maintains activity at much higher temperatures than either BA2 or the *B. amyloliquefaciens* enzyme (Figure 1B).

Structure of Native BA2 α-Amylase at 1.7 Å. The structure of BA2 was solved by conventional MIR techniques. Six isomorphous derivatives were prepared by soaking crystals of BA2 in 1−10 mM of the appropriate heavy-atom salt: chloro(2,2′:6′,2″-terpyridine)platinum(II), potassium dicyanoaurate(I), uranyl(VI) acetate, *N*-iodosuccinimide, mercury(II) chloride, and cadmium(II) acetate (phasing data not shown). The MIR phases, at 2.2 Å resolution, were improved by density-modification using DM, and this provided a readily interpretable map. The structure was refined against both 1.9 Å room-temperature data and data collected to 1.7 Å from a single crystal at 100 K at the European Synchrotron Radiation Facility.

Data collected to 1.9 Å at 298 K are 98.9% complete with an overall R_{merge} of 0.11, a mean multiplicity of 4.6 observations/reflection, and a mean $I/\sigma(I)$ of 13.2. In the highest resolution bin (1.98−1.92 Å), the data are 97.4% complete with an R_{merge} of 0.18 and a mean $I/\sigma I$ of 7.3. The unusually high R_{merge} values for the data result from poor estimation of the strong low-resolution terms due to a detector error. All further discussion will, therefore, refer to the superior 1.7 Å data, described below, unless explicitly stated. The final 1.7 Å native (100 K) data have an R_{merge} of 0.070 and are 98.1% complete with a mean multiplicity of observation of 3.0 and a mean $I/\sigma I$ of 15.1. In the highest resolution shell (1.76−1.70 Å), the data are 98.8% complete with an R_{merge} of 0.081 and a mean $I/\sigma(I)$ of 13.

The BA2 native model, at 1.7 Å, has a crystallographic *R* value of 0.14, with a corresponding R_{free} of 0.19 using all observed data between 20 and 1.7 Å. This model shows deviations from stereochemical target values of 0.010 Å for 1−2 bonds and 0.028 Å for the 1−3 bonding distance. Data and model quality parameters for the native and complex BA2 structures are shown in Table 1. There is a single outlier

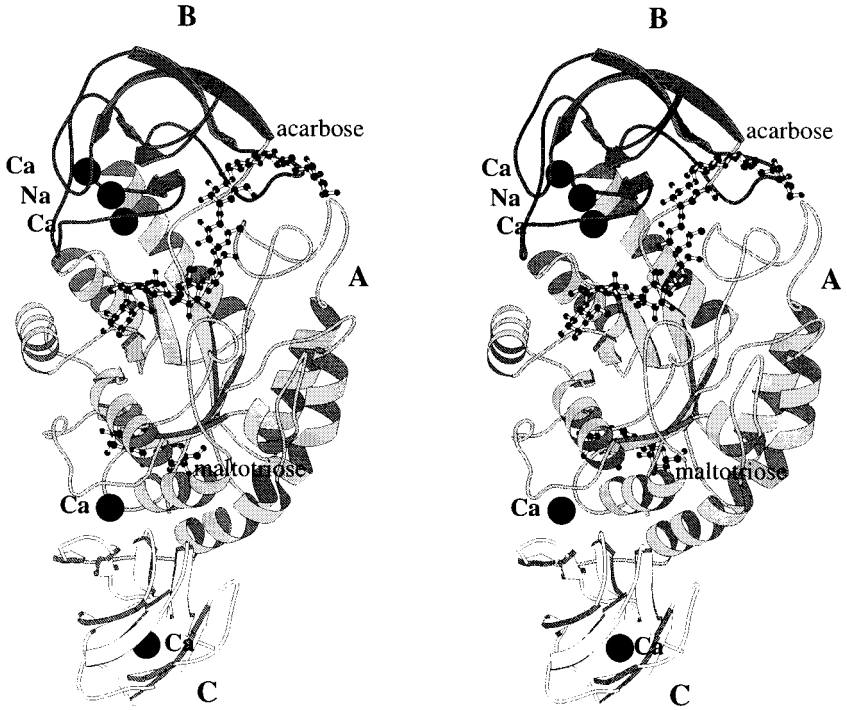

FIGURE 2: (A) Schematic protein "cartoon" of the BA2 α-amylase in complex with an acarbose-derived decasaccharide inhibitor. Active site residues and the inhibitor are shown in ball-and-stick representation. The position of the bound maltotriose, as observed in an additional complex, is superimposed for reference. This figure was prepared using MOLSCRIPT (*37*).

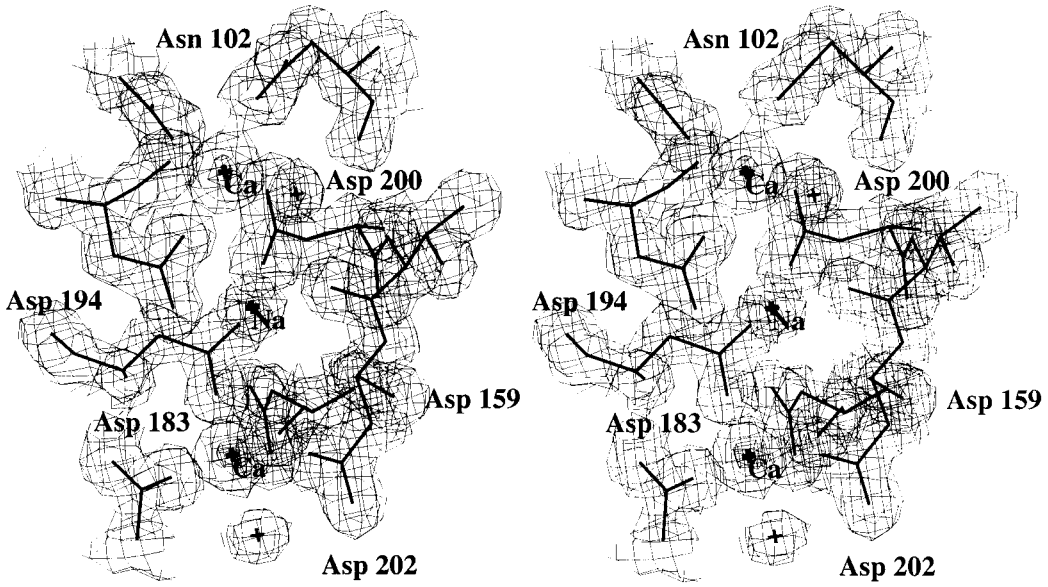

FIGURE 3: Observed electron density for the $Ca^{2+}-Na^{+}-Ca^{2+}$ cluster in BA2. The map shown is a maximum-likelihood/σ_A-weighted $2F_{obs} - F_{calc}$ synthesis at 1.7 Å resolution contoured at a level of 0.6 electron/Å^3.

on the Ramachandran plot, Tyr148, as was also seen in the Ca^{2+}-depleted *B. lichiniformis* α-amylase (*9*). This residue lies in well-defined electron density in a type II β-turn as residue $i+2$, a position more usually associated with a glycine. The model also contains a single cis-peptide in a type IV β-turn between Trp184 and Glu185. In none of the BA2 structures, described here, do we see evidence for a chloride ion in the active center as was reported for the calcium-depleted BLA α-amylase (*9*).

BA2 amylase is made up of 483 amino acids with a molecular mass of 55 kDa. The structure is made up of three globular domains ordered A, B, and C with respect to sequence, which lie in an approximately linear arrangement in the order B, A, C (Figure 2). Residues 1−103 and 206−395 make up domain A, an excursion between barrel-strands β-3 and helix α-3 (residues 104−205) forms domain B, and residues 396−483 complete domain C. This gives rise to an elongated molecule, the longest axis being some 85 Å. The widest point perpendicular to this axis is approximately 50 Å and spans the central A domain. The A domain is a standard $(\beta/\alpha)_8$ barrel as described for all other members of family 13 (for review, see ref *18*). The $(\beta/\alpha)_8$ barrel is decorated at the C-terminal end by the catalytic apparatus which comprises Asp231 from strand 4, Glu261 from strand 5, and Asp328 from strand 7. The overall structure of the chimeric α-amylase BA2 is extremely similar to that

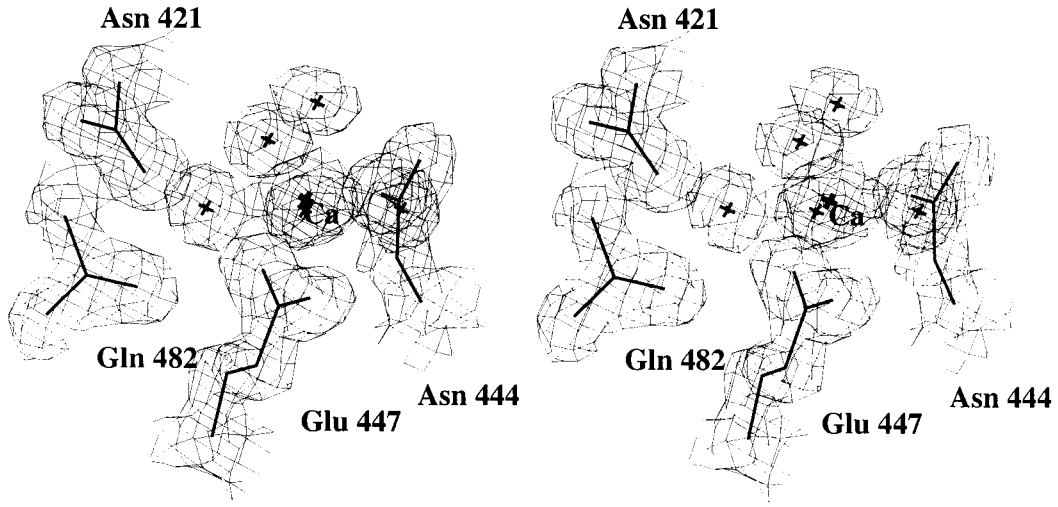

FIGURE 4: Observed electron density for the C domain Ca^{2+} ion. The map shown is a maximum-likelihood/σ_A-weighted $2F_{obs} - F_{calc}$ synthesis at 1.7 Å resolution contoured at a level of 0.6 electron/Å^3.

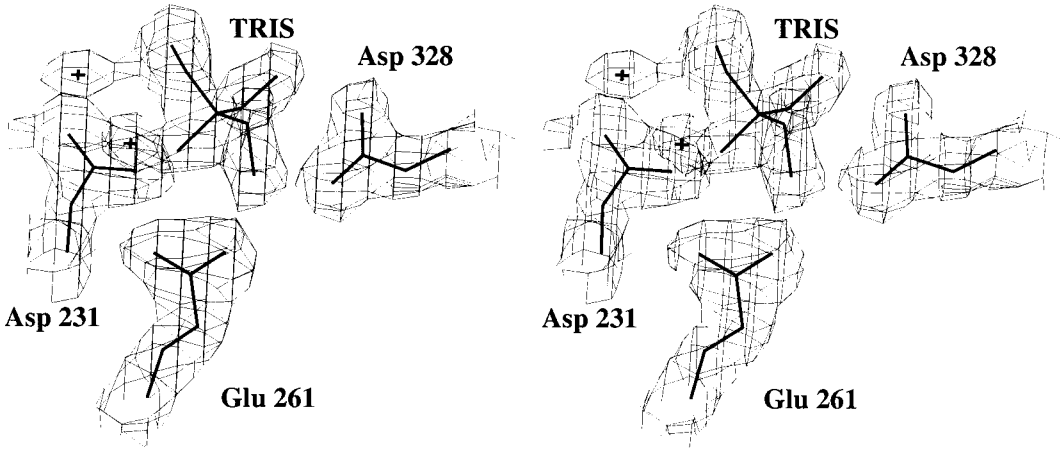

FIGURE 5: Observed electron density for TRIS bound to the active site of BA2. The map shown is a maximum-likelihood/σ_A-weighted $2F_{obs} - F_{calc}$ synthesis at 2.2 Å resolution contoured at a level of 0.44 electron/Å^3.

described previously for the *B. licheniformis* amylase (*9*), which donates residues 301−483 of the BA2 chimera: 481 equivalent Cα atoms overlap with an rms of just 0.47 Å using LSQMAN (*32*).

Calcium Binding to BA2. BA2 contains four calcium ions. Two of these are tightly bound at the interface between the A and B domains, flanking a tightly bound sodium (Figure 3). This cluster is extremely similar to that described for a mutant BLA amylase (*33*) despite the fact that in BA2 the ligands reside in the N-terminal portion of the chimera which was derived from *B. amyloliquefaciens*, confirming that these sites are conserved between these closely related organisms. The third calcium site (not shown) is found at the interface between the A and C domains and is essentially identical to that described for the BLA enzyme alone (*33*) (not shown). Elements of the calcium coordination sphere of this calcium, the main-chain carbonyls of Gly300 and Tyr302, are adjacent to the point of crossover of the chimera, so it is important that this region remains isomorphous with BLA. In addition, BA2 contains a fourth metal site, most likely a calcium, but possibly also a potassium ion, not described for BLA. This lies on the C domain and hence is formed by the *B. licheniformis* portion of the chimera alone, so it is intriguing that this site does not occur in the reported BLA structure. This metal, which refines with a temperature factor of 10.6 Å^2 when modeled as calcium, has eight ligands: five water molecules, the side-chain carbonyl oxygen from Asn444, and a bidentate interaction with the carboxylate of Glu447 (Figure 4). The second coordination sphere involves Gln482 and Asn421. These residues lie on the "upper" face of the β-sandwich, with the first coordination shell ligands, Asn444 and Glu447, lying on the lower face so the calcium appears to stabilize the two faces of the β-barrel. In BA2, there is no evidence for the low-occupancy, inhibitory, calcium site observed in the active site of some fungal α-amylases (*4*, *5*).

Structure of the TRIS/Maltotriose Complexes at 2.2 Å. X-ray data for several potential complexes of BA2 were collected in the presence of TRIS buffer. Unfortunately, TRIS acts as a competitive inhibitor for many glycoside hydrolases since its hydroxyl functions mimic those found on a sugar ring and its positive charge mimics that found in the oxocarbenium ion-like transition state. Indeed, a single molecule of TRIS was found in the active site of the complexes (Figure 5), with its positively charged nitrogen atom binding to the catalytic nucleophile, Asp231, as would be predicted. The presence of TRIS prevented oligosaccharide binding along the active-site canyon in crystallographic soaking experiments. An alternative maltooligosaccharide binding site was discovered on the N-terminal face of the

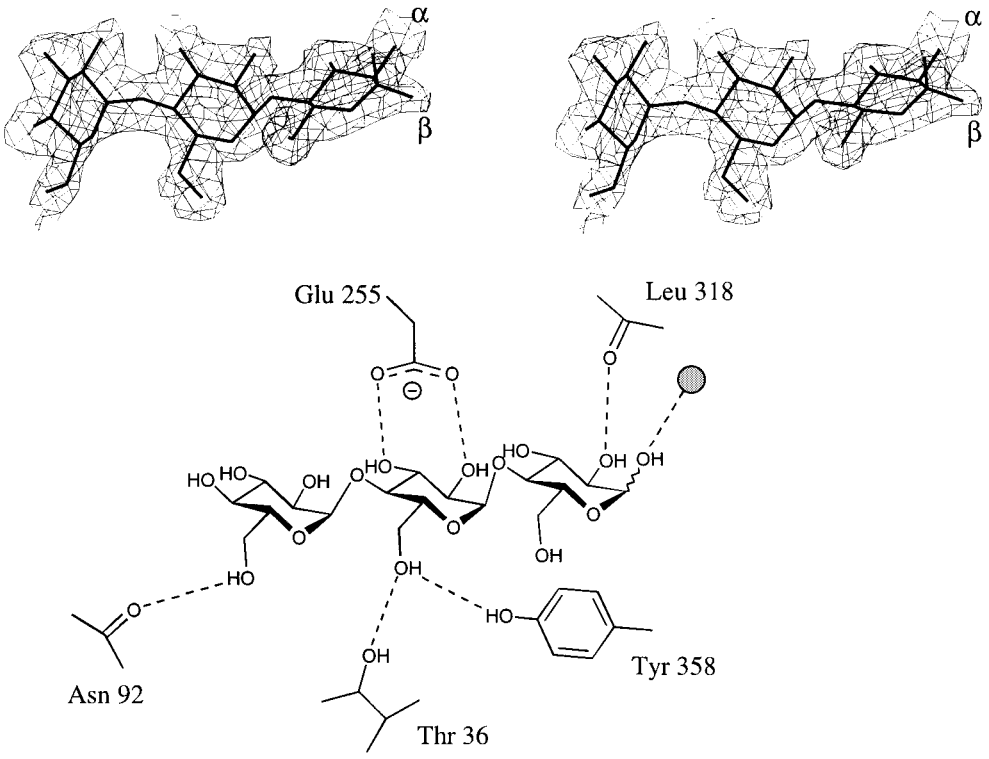

FIGURE 6: (A) Electron density for maltotriose binding to the N-terminal side of the $(\beta/\alpha)_8$ barrel. The map shown is a maximum-likelihood/σ_A-weighted $2F_{obs} - F_{calc}$ synthesis at 2.2 Å resolution contoured at a level of 0.44 electron/Å^3. (B) Schematic figure of the interactions of maltotriose with BA2. Hydrogen bonds less than 3.2 Å are indicated. Water molecules are shown as shaded spheres.

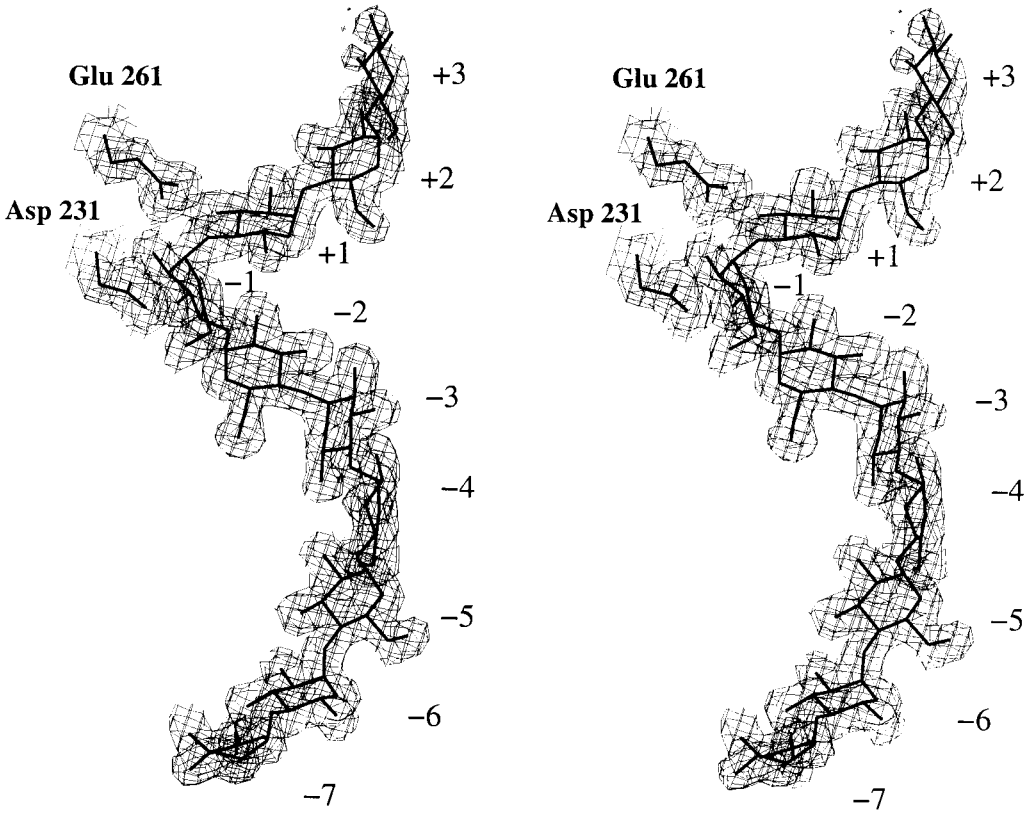

FIGURE 7: Observed electron density for the acarbose-derived tetrasaccharide, contoured at 0.44 electron/Å^3. The map shown is a $2F_{obs} - F_{calc}$ map, calculated with phases generated *prior* to the incorporation of this ligand in the refinement.

$(\beta/\alpha)_8$ barrel (Figure 6A). This site makes no lattice contacts with any symmetry-related molecules, suggesting that it is a genuine maltooligosaccharide binding site and is not an artifact of adventitious interactions. We are not aware of any equivalent binding site being reported for a member of the α-amylase superfamily, previously. Its biological function remains unclear, but it may simply play a role in locating the enzyme on the starch granule. This site is occupied with

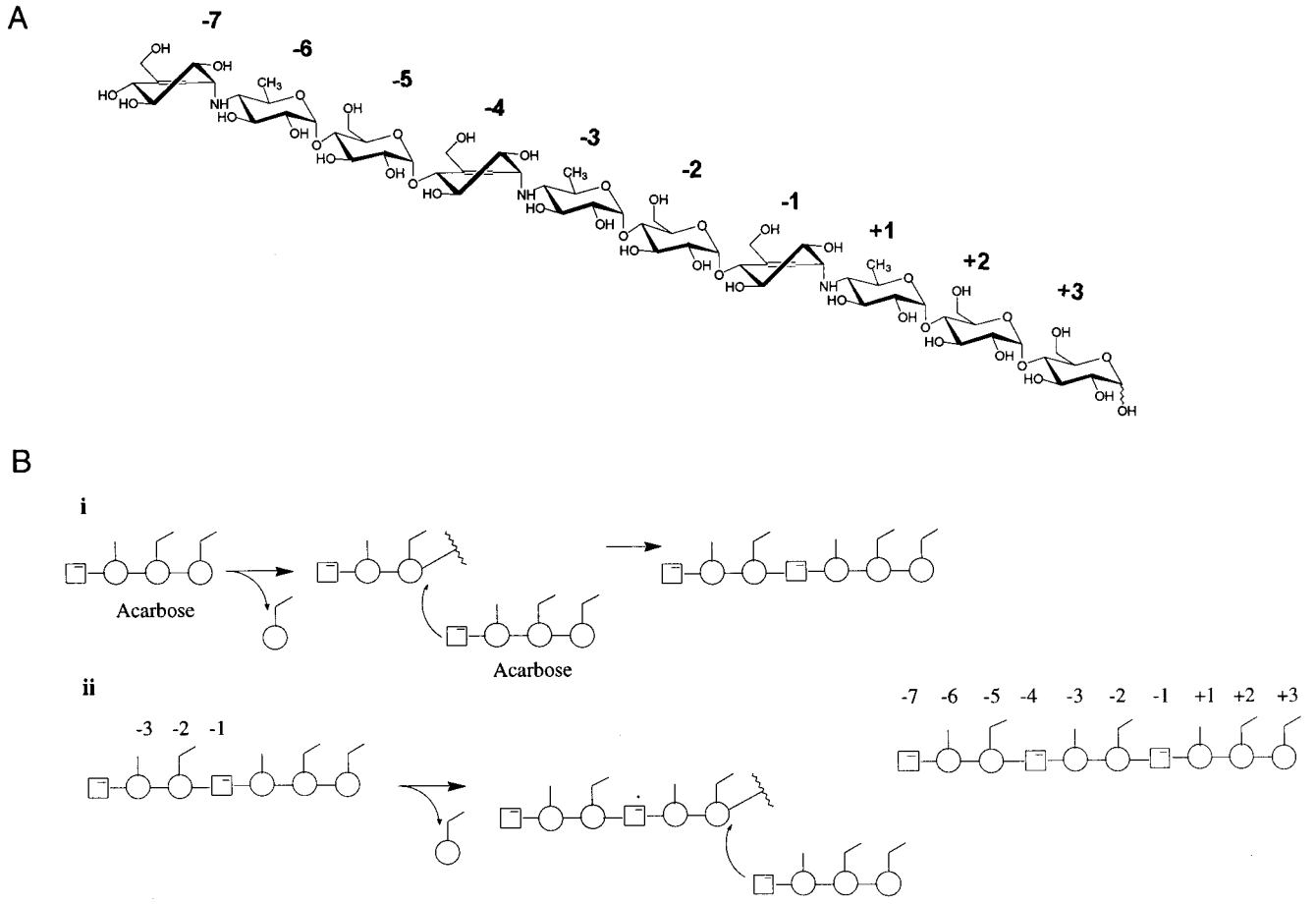

FIGURE 8: (A) Schematic representation of the acarbose-derived decasaccharide. (B) Two-step processive transglycosylation scheme for the formation of the acarbose-derived decasaccharide. (i) Acarbose first forms a glycosyl-enzyme internediate with release of glucose. This reacts with a second molecule of acarbose acting as the acceptor. (ii) The newly formed heptasaccharide migrates through the active site. A second covalent intermediate is formed with release of the reducing-end glucose as leaving group, and this is again intercepted by a further acarbose acceptor to form a decasaccharide.

a maltotriose species in data collected from crystals soaked with either maltohexaose or maltoheptaose. The reducing-end glucose unit of the trisaccharide binds through a stacking interaction with Tyr358 and by a hydrogen bond to the main-chain carbonyl oxygen of Leu318. The central sugar makes extensive hydrogen bonds to protein from its O(2) and O(3) hydroxyls to Glu255 and from its O(6) hydroxyl to both the hydroxyl of Tyr358 and the OG of Thr36. The nonreducing end sugar makes just a single direct hydrogen bond to protein to the main-chain carbonyl of Asn92 (Figure 6B).

Structure of the Acarbose-Derived Decasaccharide at 1.9 Å. The structure of BA2 in complex with the tetrasaccharide inhibitor acarbose was solved at a resolution of 1.9 Å. In the initial electron-density maps, it was clear that the tetrasaccharide inhibitor was bound as an apparent decasaccharide species (Figure 7). Acarbose complexes of α-amylases are frequently observed bound as longer species, resulting either from transglycosylation or from an overlap of tetrasaccharides (see *6*, *10*, *16*, *34*, *35*). In the BA2−acarbose complex, the decasaccharide spans the −7 to +3 subsites of the enzyme.

The tetrasaccharide acarbose is a member of the trestatin family of inhibitors originally isolated from *Streptomycetes* and developed for the treatment of sugar metabolism disorders (*36*). It possesses a nonreducing end pseudodisaccharide, consisting of a valienamine moiety linked by a nonhydrolyzable α-1,4 *N*-glycosidic bond to a 6-deoxyglucoside, which is in turn linked to maltose. The strong inhibitory power, may be attributed to the half-chair/envelope conformation of the valienamine which mimics the oxocarbenium ion-like transition state, recently quantified using free energy relationships (*34*). The two distinguishing features of acarbose are the unsaturated ring at the nonreducing end, whose double bond across C(5)−C(7) induces planarity of C(4)−C(5)−C(7)−C(1), and the absence of the O(6) hydroxyl in the adjacent 6-deoxypyranoside (Figure 8A). Particular care was taken during the refinement of the acarbose-derived decasaccharide in order to identify potential half-chair rings or 6-deoxy sugars. All O(6) hydroxyls were omitted from refinement, no torsion angle restraints were applied to the pyranosides, and $2F_{obs} - F_{calc}$ electron density maps, such as Figure 7, were calculated using phases generated prior to the incorporation of the ligand. This refinement and unbiased electron density maps clearly reveal the presence of three 6-deoxy sugars plus three half-chair unsaturated rings (Figure 8A). Together, these features indicate the presence of a single covalent species generated by two successive transglycosylation events "in-crystal". This decasaccharide binds around the surface of the enzyme in a spiral manner resembling the structure of the starch helix (Figure 9).

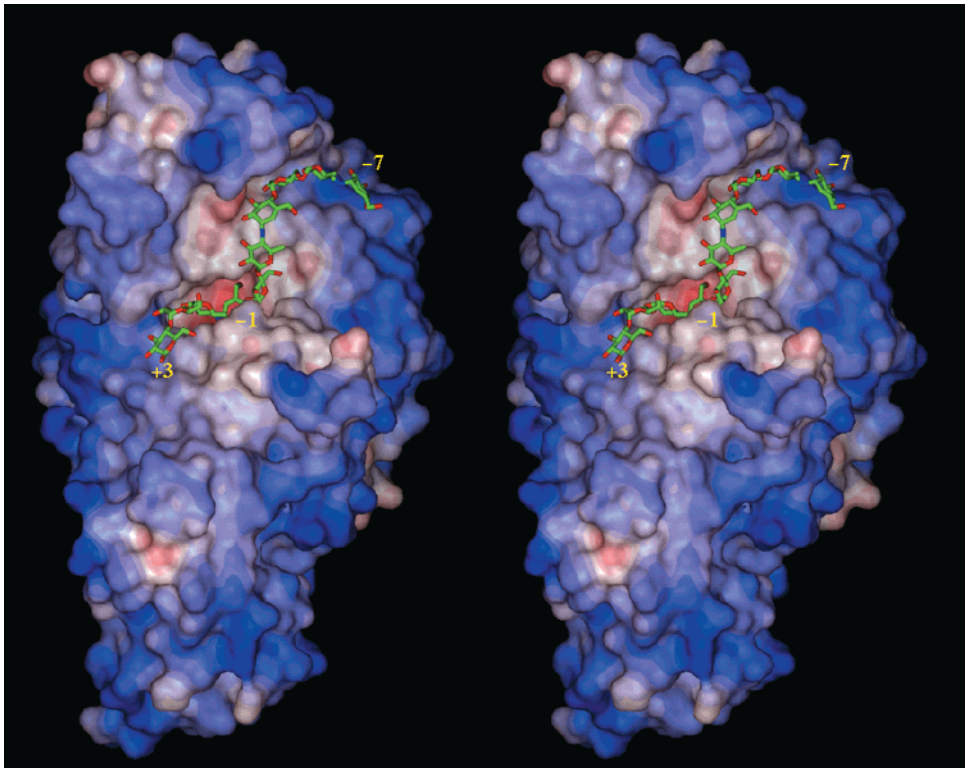

FIGURE 9: Electrostatic surface representation of BA2 amylase in complex with an acarbose-derived decasaccharide. The figure is in divergent (wall-eyed) stereo.

Family 13 of the glycoside hydrolases performs catalysis with net retention of configuration. The mechanism is a double displacement (*20*) in which the formation of a covalent glycosyl-enzyme intermediate is flanked by oxocarbenium ion-like transition states. This covalent intermediate may be trapped by a variety of means (see, for example, refs *21*−*23*) and has recently been analyzed by X-ray crystallography (*17*). The covalent glycosyl-enzyme intermediate either may be attacked by a nucleophilic water molecule in a hydrolytic reaction, or may be intercepted by a non-water molecule, frequently a second sugar unit, in a transglycosylation reaction. The presence of three 6-deoxy sugars plus three half-chair unsaturated rings demonstrates that the acarbose-derived decasaccharide species is created by two such transglycosylations. A covalent glycosyl-enzyme intermediate is first formed, with release of glucose, and this is reacted with a second molecule of acarbose acting as the acceptor. Following procession of this newly formed heptasaccharide down the substrate binding cleft, a second covalent intermediate is formed, and a second acarbose acceptor completes the formation of the decasaccharide (Figure 8B). In the final binding mode, the inhibitor occupies the −7 to +3 sites, with an acarbose moiety spanning −1 to +4 as expected. The −1 subsite unsaturated ring is in a conformation between $^2H_3$ and ^2E, with C2 0.67 Å above the plane defined by C4−C5−C7−C1 and C3 0.17 Å below.

Further support for a model involving transglycosylation comes from data collected, to 2.8 Å, on a catalytically deficient mutant of BA2. The mutation of the catalytic acid, E261A, should, by analogy with other systems (*17*, *34*), be unable to perform transglycosylation due to the absence of the base function to activate the acceptor species. The E261A−acarbose complex indeed reveals binding of a single tetrasaccharide species with no evidence for transglycosylation. This acarbose molecule binds in the −7 to −4 subsites, and not in −1 to +3 as expected, and is highly disordered (data not shown). The absence of an extended species in a catalytically deficient enzyme provides support for the transglycosylation of these species observed in catalytically competent enzymes. It also demonstrates that acarbose is able to bind to the other subsites in a substrate, as opposed to the transition-state, mimicking mode.

The ensemble of BA2 structures provides further insight into the structure and function of starch-degrading enzymes. Ten of the enzyme subsites are mapped, and a novel maltotrioside binding site is revealed on the "wrong" face of the $(\beta/\alpha)_8$ barrel. Unbiased electron density strongly suggests a two-step processive transglycosylation in-crystal. The chimeric nature of this enzyme also reveals the potential for gene shuffling to generate novel enzymes for industrial applications.

REFERENCES

1. Henrissat, B. (1991) *Biochem. J. 280*, 309−316.
2. Henrissat, B., and Bairoch, A. (1993) *Biochem. J. 293*, 781−788.
3. Henrissat, B., and Bairoch, A. (1996) *Biochem. J. 316*, 695−696.
4. Swift, H. J., Brady, L., Derewenda, Z. S., Dodson, E. J., Dodson, G. G., Turkenburg, J. P., and Wilkinson, A. J. (1991) *Acta Crystallogr. B47*, 535−544.
5. Boel, E., Brady, L., Brzozowski, A. M., Derewenda, Z., Dodson, G. G., Jensen, V. J., Petersen, S. B., Swift, H., Thim, L., and Woldike, H. F. (1990) *Biochemistry 29*, 6244−6249.
6. Qian, M., Haser, R., Buisson, G., Duée, E., and Payan, F. (1994) *Biochemistry 33*, 6284−6294.
7. Kadziola, A., Sogaard, M., Svensson, B., and Haser, R. (1998) *J. Mol. Biol. 278*, 205−217.

8. Rydberg, E. H., Sidhu, G., Vo, H. C., Hewitt, J., Cote, H. C., Wang, Y., Numao, S., MacGillivray, R. T., Overall, C. M., Brayer, G. D., and Withers, S. G. (1999) *Protein Sci. 8*, 635−643.
9. Machius, M., Wiegand, G., and Huber, R. (1995) *J. Mol. Biol. 246*, 545−559.
10. Dauter, Z., Dauter, M., Brzozowski, A. M., Pedersen, A., Wilson, K. S., and Davies, G. J. (1999) *Biochemistry 38*, 8385−8392.
11. Aghajari, N., Feller, G., Gerday, C., and Haser, R. (1998) *Structure 6*, 1503−1516.
12. Aghajari, N., Feller, G., Gerday, C., and Haser, R. (1998) *Protein Sci. 7*, 564−572.
13. Klein, C., Hollender, J., Bender, H., and Schulz, G. E. (1992) *Biochemistry 31*, 8740−8746.
14. Schmidt, A. K., Cottaz, S., Driguez, H., and Schulz, G. E. (1998) *Biochemistry 37*, 5909−5915.
15. Strokopytov, B., Penninga, D., Roseboom, H. J., Kalk, K. H., Dijkhuizen, L., and Dijkstra, B. W. (1995) *Biochemistry 34*, 2234−2240.
16. Strokopytov, B., Knegtel, R. M. A., Penninga, D., Rozeboom, H. J., Kalk, K. H., Dijkhuizen, L., and Dijkstra, B. W. (1996) *Biochemistry 35*, 4241−4249.
17. Uitdehaag, J. C. M., Mosi, R., Kalk, K. H., van der Veen, B. A., Dijkhuizen, L., Withers, S. G., and Dijkstra, B. W. (1999) *Nat. Struct. Biol. 6*, 432−436.
18. Svensson, B. (1994) *Plant Mol. Biol. 25*, 141−157.
19. Davies, G., Sinnott, M. L., and Withers, S. G. (1997) in *Comprehensive Biological Catalysis* (Sinnott, M. L., Ed.) pp 119−209, Academic Press, London.
20. Koshland, D. E. (1953) *Biol. Rev. 28*, 416−436.
21. Braun, C., Brayer, G. D., and Withers, S. G. (1995) *J. Biol. Chem 270*, 26778−26781.
22. McCarter, J. D., and Withers, S. G. (1996) *J. Biol Chem 271*, 6889−6894.
23. Mosi, R., He, S., Uitdehaag, J., Dijkstra, B. W., and Withers, S. G. (1997) *Biochemistry 36*, 9927−9934.
24. Otwinowski, Z. (1993) in *Data Collection and Processing: proceedings of the CCP4 study weekend* (Sawyer, L., Isaacs, N., and Bailey, S., Eds.) Science and Engineering Research Council, Daresbury, U.K.
25. Otwinowski, Z., and Minor, W. (1997) in *Methods in Enzymology: Macromolecular Crystallography, Part A* (C W Carter, J., and Sweet, R. M., Eds.) pp 307−326, Academic Press, London and New York.
26. Collaborative Computational Project Number 4 (1994) *Acta Crystallogr. D50*, 760−763.
27. Cowtan, K. D., and Main, P. (1996) *Acta Crystallogr. D49*, 148−157.
28. Jones, T. A., Zou, J.-Y., Cowan, S. W., and Kjeldgaard, M. (1991) *Acta Crystallogr. A47*, 110−119.
29. Brünger, A. T. (1992) *Nature 355*, 472−475.
30. Murshudov, G. N., Vagin, A. A., and Dodson, E. J. (1997) *Acta Crystallogr. D53*, 240−255.
31. Nielsen, J. P., Beier, L., Otzen, D., Borchert, T. V., Frantzen, H. B., Andersen, K. V., and Svendsen, A. (1999) *Eur. J. Biochem. 264*, 816−824.
32. Kleywegt, G. J., and Jones, T. A. (1994) *ESF/CCP4 Newslett. 31*, 9−14.
33. Machius, M., Declerck, N., Huber, R., and Wiegand, G. (1998) *Structure 6*, 281−92.
34. Mosi, R., Sham, H., Uitdehaag, J. C., Ruiterkamp, R., Dijkstra, B. W., and Withers, S. G. (1998) *Biochemistry 37*, 17192−17198.
35. Brzozowski, A. M., and Davies, G. J. (1997) *Biochemistry 36*, 10837−10845.
36. Schmidt, D. D., Frommer, W., Junge, B., Müller, L., Wingender, W., and Truscheit, E. (1981) in *First international symposium on acarbose* (Creutzfeldt, W., Ed.) pp 5−15, Excerpta Medica, Amsterdam.
37. Kraulis, P. J. (1991) *J. Appl. Crystallogr. 24*, 946−950.

BI0000317